IMMUNOLOGY

Fc receptor–like 1 intrinsically recruits c-Abl to enhance B cell activation and function

Xingwang Zhao[1]*, Hengyi Xie[1]*, Meng Zhao[1]*, Asma Ahsan[2], Xinxin Li[1], Fei Wang[3], Junyang Yi[1], Zhiyong Yang[4], Chuan Wu[5], Indu Raman[6], Quan-Zhen Li[6†], Tae Jin Kim[7†], Wanli Liu[1†]

B cell activation is regulated by the stimulatory or inhibitory co-receptors of B cell receptors (BCRs). Here, we investigated the signaling mechanism of Fc receptor-like 1 (FcRL1), a newly identified BCR co-receptor. FcRL1 was passively recruited into B cell immunological synapses upon BCR engagement in the absence of FcRL1 cross-linking, suggesting that FcRL1 may intrinsically regulate B cell activation and function. BCR cross-linking alone led to the phosphorylation of the intracellular Y_{281}ENV motif of FcRL1 to provide a docking site for c-Abl, an SH2 domain-containing kinase. The FcRL1 and c-Abl signaling module, in turn, potently augmented B cell activation and proliferation. FcRL1-deficient mice exhibited markedly impaired formation of extrafollicular plasmablasts and germinal centers, along with decreased antibody production upon antigen stimulation. These findings reveal a critical BCR signal-enhancing function of FcRL1 through its intrinsic recruitment to B cell immunological synapses and subsequent recruitment of c-Abl upon BCR cross-linking.

INTRODUCTION

The establishment of appropriate humoral immunity is based on strict regulation of B cell activation. More than 20 immunoglobulin (Ig) superfamily receptors have been identified on the surface of B cells, and these receptors perform either positive or negative regulatory functions in B cell activation (*1*). The cell surface expression of B cell receptor (BCR), which contains a membrane-bound Ig molecule that noncovalently associates with the CD79A-CD79B heterodimer, is essential for B cell survival and function (*2*). Upon antigen binding, BCRs oligomerize to microclusters (*3*), accompanied by tyrosine phosphorylation within immunoreceptor tyrosine-based activation motifs (ITAMs) in the cytoplasmic domains of the CD79A-CD79B heterodimer by Src family kinases (*4*, *5*). The phosphorylated ITAMs serve as docking sites for Syk kinase (*6*, *7*), which further recruits a series of downstream signaling molecules, including phospholipase C–γ2 (PLC-γ2) (*8*), Bruton's tyrosine kinase (BTK) (*9*), and Vav, alongside adaptor molecules, such as B cell linker (BLNK) (*10*), leading to the formation of the Syk-derived membrane-proximal signalosome (*11*). In addition, the BCR signalosome also recruits the p85α/p110δ isoform of phosphatidylinositol 3-kinase (PI3K) to promote B cell proliferation (*12*). Phosphatidylinositol (4,5)-bisphosphate (PIP_2) and phosphatidylinositol (3,4,5)-trisphosphate (PIP_3) equilibrium governed by PI3K and PTEN (phosphatase and tensin homolog) regulates B cell activation through Dock2, which remodels the F-actin cytoskeleton and controls the growth of BCR microclusters (*13*, *14*). This cytoskeletal rearrangement promotes a two-phase response of B cells in which they first spread over the antigen-bearing surface and then contract, thereby collecting BCR and antigen-coupled microclusters into the center of the B cell immunological synapse (*15*).

The initiation of B cell activation is strictly regulated by activating co-receptors, including CD19, and inhibitory co-receptors, including FcγRIIB. CD19 is known for its ability to bind PI3K and Vav through ITAMs within its cytoplasmic tail and to promote the recruitment of lipid rafts into the immunological synapse (*16*). In contrast, FcγRIIB, which recognizes IgG Fc domains within immune complexes and bears cytoplasmic immunoreceptor tyrosine-based inhibitory motifs, recruits Src homology 2-containing inositol-5′-phosphatase to specifically remove the phosphate from the 5′ position of PIP_3 to produce $PI(3,4)P_2$, thereby negatively regulating the PI3K pathway to down-regulate BCR signaling (*17*). Live cell imaging studies also revealed that the transmembrane domain of FcγRIIB can inhibit B cell activation by blocking the colocalization of BCR and CD19 microclusters within the B cell immunological synapse (*18*, *19*).

In addition to the classic Fc receptors (FcRs), including FcγRIIB, FcR-like (FcRL) molecules, a new family of Ig domain–containing type I membrane proteins sharing the same ancestor with FcRs, have been recently identified (*20*). To date, a total of eight human and six mouse FcRL family members have been identified. Human B cells express FcRL1 to FcRL5 on the plasma membrane, whereas mouse B cells only express FcRL1 and FcRL5 (*20*). FcRL1 to FcRL5 all have one or more immunoreceptor tyrosine-based regulatory motifs in their cytoplasmic tails. Among them, FcRL1 is selectively expressed on the surface of $CD19^+$ mature B cells. Quantitative reverse transcription polymerase chain reaction (RT-PCR) demonstrated that FcRL1 expression begins in pre–B cells and that its expression level increases highly in naïve and memory B cells and decreases in pre–germinal center (pre-GC) and GC B cell and plasma cell populations

[1]MOE Key Laboratory of Protein Sciences, Center for Life Sciences, Collaborative Innovation Center for Diagnosis and Treatment of Infectious Diseases, School of Life Sciences, Beijing Key Lab for Immunological Research on Chronic Diseases, Institute for Immunology, Tsinghua University, Beijing 100084, China. [2]Biochemistry and Structural Biology Lab, Department of Biology, Syed Babar Ali School of Science and Engineering, Lahore University of Management of Sciences (LUMS) Lahore, Pakistan. [3]Natural Products Research Center, Chengdu Institute of Biology, Chinese Academy of Science, Chengdu 610041, China. [4]Cardiovascular Research Institute, University of California, San Francisco, San Francisco, CA 94143, USA. [5]Experimental Immunology Branch, National Cancer Institute, U.S. National Institutes of Health, Bethesda, MD 20851, USA. [6]Department of Immunology and Internal Medicine, IIMT Microarray Core Facility, University of Texas Southwestern Medical Center, Dallas, TX 75390, USA. [7]Division of Immunobiology, School of Medicine, Sungkyunkwan University, 2066 Seobu-ro, Jangan-gu, Suwon 16419, Republic of Korea.
*These authors contributed equally to this work.
†Corresponding author. Email: liulab@tsinghua.edu.cn (W.L.); tjkim@skku.edu (T.J.K.); quan.li@utsouthwestern.edu (Q.-Z.L.)

(*21*). Although the ligand for FcRL1 has not been identified, the presence of two ITAM-like motifs within its intracellular domain has suggested its positive function in B cell activation. In vitro studies revealed that the antibody-mediated cross-linking of the extracellular domain of FcRL1 resulted in the phosphorylation of its intracellular tyrosine residues and that the augmentation of antigen binding induced Ca^{2+} mobilization and B cell proliferation (*21*), suggesting the role of FcRL1 as a positive regulator of B cell activation. However, few studies have addressed the signaling pathways controlled by the ITAM-like motifs within the intracellular domain of FcRL1 and whether the role of FcRL1 in B cell activation is strictly dependent on ligand binding. Furthermore, the physiological function of FcRL1 in B cell development and humoral immune response is not investigated. To address these questions, we generated FcRL1 knockout (KO) cell line and mice and performed combined biochemical, biophysical, and live cell imaging experiments to investigate the function of FcRL1 in the regulation of B cell activation and antibody response.

RESULTS

FcRL1 deficiency impaired B cell activation in the absence of FcRL1 ligation

BCRs are evenly distributed on the surface of the plasma membrane in quiescent B cells. Upon stimulation by membrane-bound antigens, BCRs oligomerize to form microclusters and aggregate in B cell immunological synapses, serving as the platform for BCR signaling and antigen internalization (*22*). The level of synaptic accumulation of BCRs is proportional to the strength of BCR activation (*23*). To investigate the function of FcRL1 in B cell activation, we generated FcRL1-deficient CH27 (CH27-FcRL1-KO) cells using the CRISPR-Cas9 system with a single-guide RNA (sgRNA) targeting to the third exon of the FcRL1 gene (fig. S1A) (*24*). We confirmed the KO efficiency by Western blotting (fig. S1, A to D). Then, we stimulated CH27–wild-type (WT) and CH27-FcRL1-KO cells with similar surface BCR levels (fig. S2A) with 30 nM F(ab′)2 fragment anti-mouse IgM as a surrogate antigen on the surface of planar lipid bilayers (PLBs) for 10 min. We compared the strength of BCR signaling by quantifying the amount of BCRs accumulated at synapses via total internal reflection fluorescence microscopy (TIRFM) imaging. In this study, we used the mean fluorescence intensity (mFI) of BCRs within the B cell contact interface instead of the total fluorescent intensity (TFI) for a more accurate measurement of BCR clustering because mFI, defined as TFI divided by size of the contact interface, indicates the density of BCRs within the B cell immunological synapse. The TFI is not preferred since it will simply increase during B cell spreading responses upon BCR stimulation and, thus, it is not possible to distinguish whether the increase in TFI is due to an accumulation of BCRs at the B cell contact interface or an increase in the size of the contact interface. Statistical quantification suggested that upon BCR cross-linking alone, CH27-FcRL1-KO cells exhibited notably impaired accumulation of BCRs into the B cell immunological synapse compared with CH27-WT cells (Fig. 1, A and B). Moreover, the synaptic accumulation of phosphorylated signaling molecules including Syk, BLNK, and PI3K (probed by the p85α subunit) was also markedly impaired in CH27-FcRL1-KO cells compared to CH27-WT cells (Fig. 1, C to H). To validate that these observations were due to FcRL1 deficiency rather than subordinate or off-target effects during the construction of CH27-FcRL1-KO cells, we performed rescue experiments, which revealed that exogenous FcRL1 (fig. S2A) restored the ability to accumulate BCRs and signaling molecules into the B cell immunological synapse in CH27-FcRL1-KO cells in response to antigen stimulation (Fig. 1). We also excluded the off-target effects of sgRNA by sequencing the potential off-target gene loci (fig. S3).

As CH27 cells represent a cancerous B cell line, we further validated these observations in primary B cells. FcRL1 is mainly expressed in follicular and marginal zone B cells in mouse. We thus designed two sgRNAs to disrupt the FcRL1 gene targeting the upstream 4th exon and the downstream 10th exon (fig. S1E). The FcRL1-KO mice generated using the CRISPR-Cas9 technique were backcrossed to C57BL/6 mice for at least three generations before further experiments. The deletion efficiency of FcRL1 was confirmed by Western blotting (fig. S1F) and PCR (fig. S1G). Quantitative RT-PCR also confirmed the loss of FcRL1 mRNA in splenic primary B cells from FcRL1-deficient mice (fig. S1H). As a control, the transcription of FcRL5 was not affected (fig. S1I). Moreover, we assessed potential off-target effects at putative off-target sites, but no unexpected mutations were observed in the genome (figs. S4 and S5). FcRL1 deficiency did not also affect IgM-BCR expression on the surface of primary B cells (fig. S2B). To examine the function of FcRL1 during the initiation of B cell activation, we placed WT and FcRL1-KO primary B cells on lipid bilayers presenting 30 nM F(ab′)2 anti-mouse IgM surrogate antigen for 10 min. TIRFM imaging confirmed that the synaptic accumulation of BCRs was severely impaired in FcRL1-KO primary B cells in comparison to that in WT primary B cells (fig. S6, A and B). Moreover, we used intracellular staining and TIRFM imaging to demonstrate that FcRL1 deficiency also severely impaired the synaptic accumulation of pSyk, pBLNK, and pPI3K (fig. S6, C to H).

We further validated the impaired B cell activation by measuring Ca^{2+} mobilization upon BCR stimulation. When WT and FcRL1-KO primary B cells were stimulated with F(ab′)2 anti-mouse IgM surrogate antigens (10 μg/ml), the amplitude of Ca^{2+} elevation was decreased in FcRL1-KO primary B cells compared with that in WT B cells (Fig. 2A). We also stimulated CH27-WT and CH27-FcRL1-KO cells with PC_{10}-BSA (10 phosphorylcholine moieties conjugated to bovine serum albumin) (15 μg/ml), a specific antigen for CH27 BCR (*25*), and compared the subsequent Ca^{2+} mobilization. Consistently, CH27-FcRL1-KO B cells exhibited notably reduced Ca^{2+} mobilization upon recognition of PC_{10}-BSA compared to CH27-WT cells (Fig. 2B).

We furthermore evaluated the proliferative responses of WT and FcRL1-KO primary B cells upon stimulation with F(ab′)2 anti-mouse IgM surrogate antigen (10 μg/ml). We monitored cell proliferation by detecting the fluorescence dilution of the cell labeling dye carboxyfluorescein diacetate succinimidyl ester (CFSE). FcRL1-KO primary B cells proliferated to a lower extent than WT primary B cells (Fig. 2C). Collectively, these findings suggest that FcRL1 plays a positive role in enhancing antigen binding–induced B cell activation in the absence of FcRL1 ligation with respect to BCR clustering, Ca^{2+} signaling, and proliferation.

FcRL1 was passively recruited into the B cell immunological synapse upon BCR engagement

Next, we investigated the distribution of FcRL1 molecules upon BCR engagement to explain why FcRL1 deficiency leads to impaired BCR-mediated B cell activation in the absence of FcRL1 ligation. The distribution of FcRL1 molecules was visualized by expressing the HA-FcRL1-YFP chimera receptor with the hemagglutinin (HA)

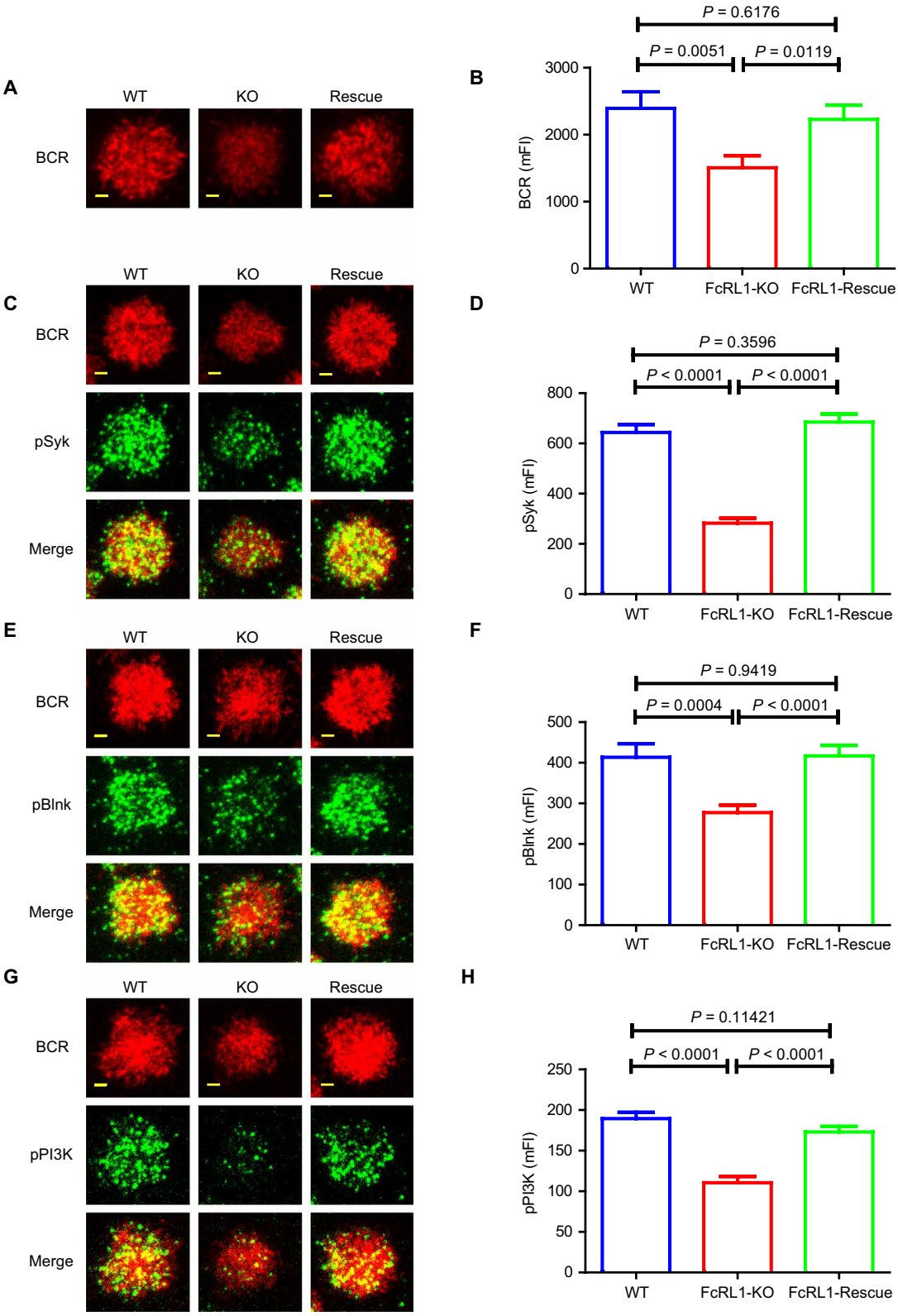

Fig. 1. FcRL1 deficiency in CH27 cells impairs B cell activation induced by antigen binding in the absence of FcRL1 ligation. Left: Representative TIRFM images showing the synaptic accumulation of BCRs (**A**) and the synaptic recruitment of pSyk (**C**), pBLNK (**E**), and pPI3K (p85α) (**G**) in CH27-WT, CH27-FcRL1-KO, and CH27-FcRL1-Rescue cells. Scale bars, 1.5 μm. Right: Statistical quantification of the synaptic accumulation of BCRs (**B**) ($n = 24$ to 27 cells) and signaling molecules of pSyk (**D**) ($n = 38$ to 75 cells), pBLNK (**F**) ($n = 39$ to 44 cells), and pPI3K (p85α) (**H**) ($n = 49$ to 59 cells) in CH27-WT, CH27-FcRL1-KO, and CH27-FcRL1-Rescue cells. Experiments were repeated three times, and data from a representative experiment are shown. Bar represents means ± SEM. Two-tailed Student's *t* tests were used for statistical comparisons.

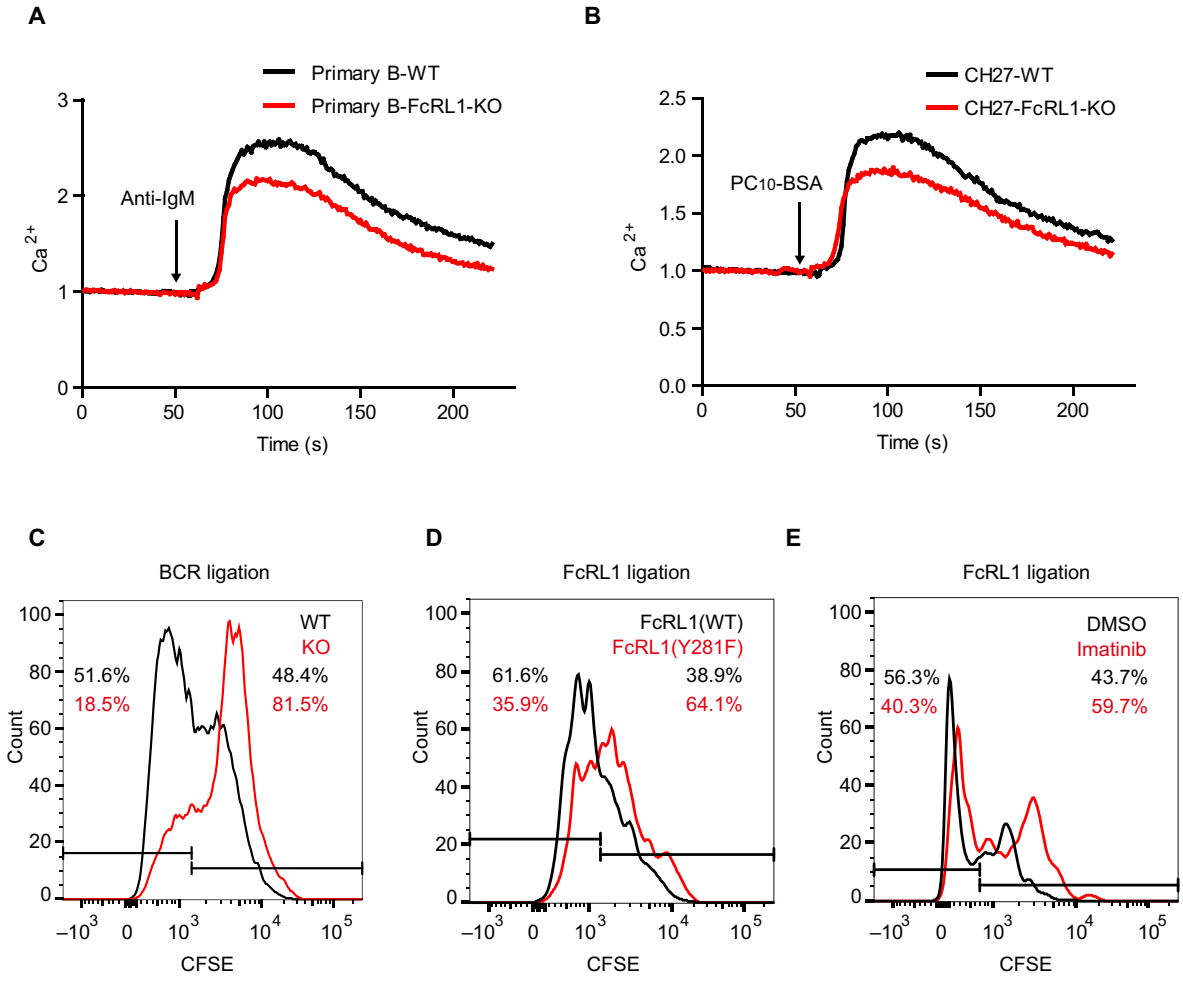

Fig. 2. FcRL1 deficiency impairs antigen binding–induced calcium mobilization and the in vitro proliferation of primary B cells. (**A** and **B**) Normalized Ca^{2+} mobilization indicated by Fluo-4–to–Fura Red ratio in primary B cells stimulated with F(ab')2 goat anti-mouse IgM (A) and in CH27 B cells stimulated with PC_{10}-BSA (B). The arrows indicate the time of antigen stimulation. Experiments were repeated three times, and data from a representative experiment are shown. (**C** to **E**) Representative proliferation profiles of mouse primary B cells at 72 hours after stimulation indicated by the decreased intensity of the proliferation marker carboxyfluorescein diacetate succinimidyl ester (CFSE). Mouse WT and FcRL1-KO primary B cells were stimulated via BCR ligation (C). Mouse FcRL1-deficient primary B cells expressing HA-FcRL1(WT)-mCherry or HA-FcRL1(Y281F)-mCherry were stimulated via FcRL1 ligation (D). Mouse FcRL1-deficient primary B cells expressing HA-FcRL1(WT)-mCherry were treated with imatinib or dimethyl sulfoxide (DMSO) via stimulated by FcRL1 ligation (E). Experiments were repeated three times, and data from a representative experiment are shown.

tag fused to the N terminus and yellow fluorescent protein (YFP) to the C terminus of FcRL1 on the surface of FcRL1-KO primary B cells. We used TIRFM to image the spatial distribution of both BCR and FcRL1 within the immunological synapse of B cells that were placed on PLBs presenting different types of cross-linking antibodies. To cross-link BCR or FcRL1 alone, we used 30 nM F(ab′)2 anti-mouse IgM or anti-HA, respectively. To ligate BCR and FcRL1 simultaneously, we applied a combination of 30 nM F(ab′)2 anti-mouse IgM and anti-HA presented on PLBs. As a negative control, we used 30 nM F(ab′)2 anti-mouse major histocompatibility complex I (MHC I). TIRFM imaging illustrated that ligation of MHC I did not induce the accumulation of either BCR or FcRL1 at the contact interface between B cells and PLBs (Fig. 3A). FcRL1 ligation strongly induced the aggregation of FcRL1 molecules, but not BCRs, in the contact zone between cells and PLBs (Fig. 3A). Unexpectedly, BCR ligation induced the accumulation of both BCR and FcRL1 at B cell immunological synapses (Fig. 3A). Further colocalization analyses of BCR and FcRL1 microclusters following the published protocol (*26*) demonstrated a high degree of codistribution of these two molecules within the B cell immunological synapse upon ligation of BCR alone or both BCR and FcRL1 (Fig. 3B). Last, as a positive control, the coligation of FcRL1 and BCR further augmented the mFIs of BCR and FcRL1 within the B cell immunological synapse compared with the ligation of either BCR or FcRL1 alone (Fig. 3, C and D). However, a careful comparison indicated that the coligation of BCR and FcRL1 did not further enhance the colocalization of these two molecules (Fig. 3B), suggesting that FcRL1 intrinsically colocalized with BCR upon BCR engagement even when FcRL1 was not cross-linked. In contrast, the ligation of FcRL1 alone led to the formation of FcRL1 microclusters, but not BCR microclusters, suggesting that B cell immunological synapse is not established or enhanced by the FcRL1 engagement (Fig. 3, C and D). We also confirmed the passive recruitment of FcRL1 into B cell immunological synapse upon BCR engagement in CH27-FcRL1-KO B cells expressing exogenous

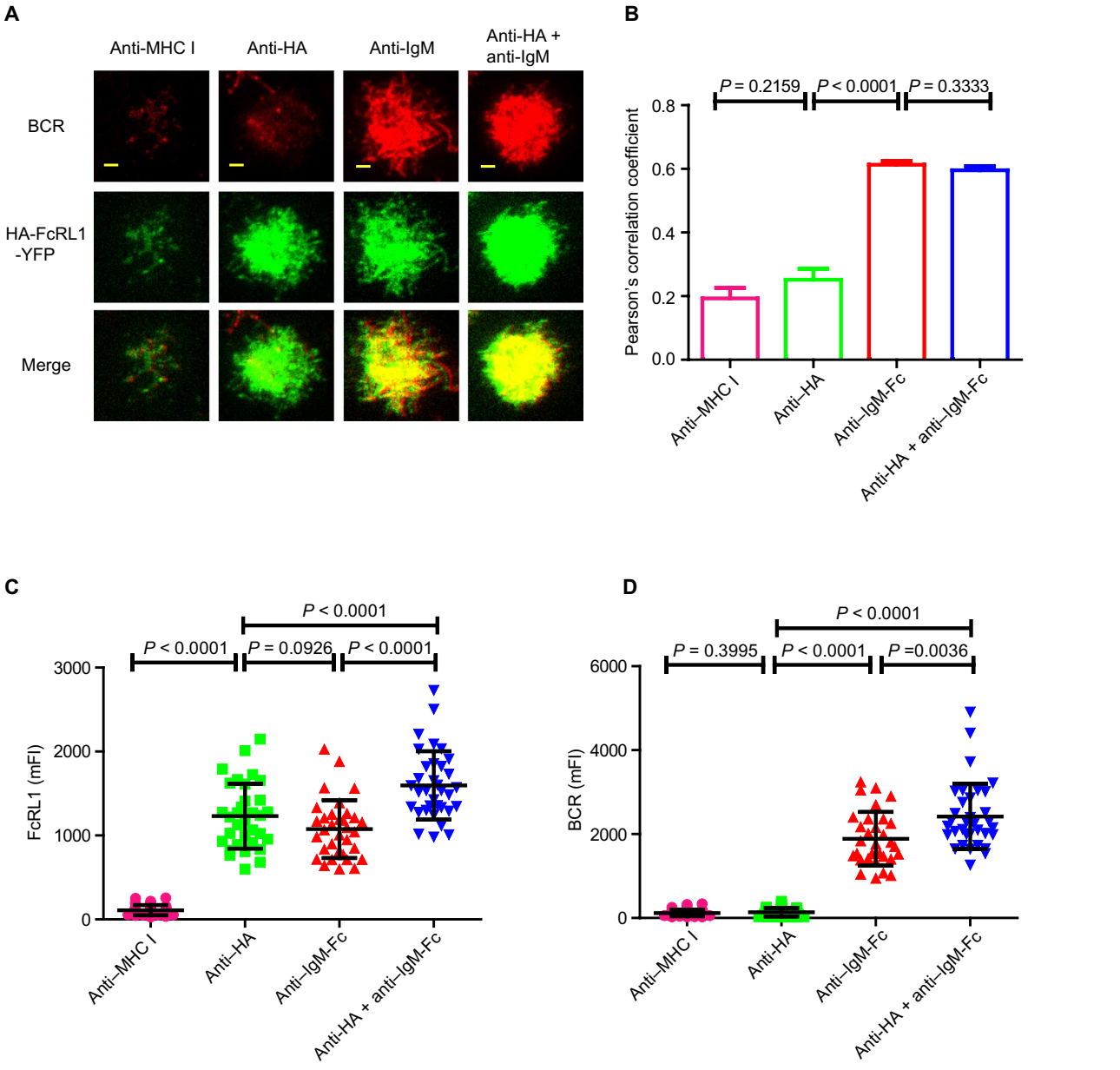

Fig. 3. FcRL1 is passively recruited into B cell immunological synapses upon BCR engagement in primary spleen B cells. (**A**) Representative TIRFM images showing the synaptic accumulation of BCR or FcRL1 in primary B cells stimulated with 30 nM F(ab')2 goat anti-mouse MHC I, 30 nM F(ab')2 rabbit anti-HA, 30 nM F(ab')2 goat anti-mouse IgM, or 30 nM F(ab')2 goat anti-mouse IgM + 30 nM F(ab')2 rabbit anti-HA. Scale bars, 1.5 μm. (**B**) Colocalization analyses of BCR and FcRL1 microclusters within B cell immunological synapses ($n = 33$ to 36 cells). Experiments were repeated three times, and data from a representative experiment are shown. Bar represents means ± SEM. Two-tailed Student's *t* tests were used for the statistical comparisons. (**C** and **D**) Statistical quantification of accumulated FcRL1 (C) ($n = 31$ to 34 cells) and BCR (D) ($n = 31$ to 35 cells) within B cell immunological synapses. Experiments were repeated three times, and data from a representative experiment are shown. Bar represents means ± SD. Each symbol represents one cell. Two-tailed Student's *t* tests were used for statistical comparisons.

HA-FcRL1-YFP (fig. S7). Collectively, these results suggest that FcRL1 molecules are passively and intrinsically recruited into BCR microclusters within B cell immunological synapses upon BCR cross-linking in the absence of FcRL1 ligation.

FcRL1 recruits c-Abl as the intracellular effector molecule

To investigate the downstream signaling mechanism of the FcRL1-mediated enhancement of BCR signaling, we aligned the amino acid sequences of the FcRL1 cytoplasmic tails from all species available in the UniProt database and identified three evolutionarily conserved tyrosine-based motifs at positions Y_{281}ENV, Y_{293}SLV, and Y_{339}EDA (fig. S8). Previous studies revealed that FcRL1 ligation induced tyrosine phosphorylation within the cytoplasmic tail (*21*). However, the tyrosine residues that are phosphorylated in response to FcRL1 ligation and downstream signaling molecules that bind to the phosphorylated tyrosine motif(s) of the FcRL1 tail remain unknown. We thus performed a database search for signaling proteins with SH2 domains that potentially bind to each of these three tyrosine-based

motifs. One of the best fits for the Y_{281}ENV motif was the SH2 domain of c-Abl, which prefers asparagine at position +2 C-terminal to the phosphorylated tyrosine residue (*27*).

Next, to address whether the phosphorylated Y_{281}ENV motif could serve as the docking site for the c-Abl–SH2 domain, we analyzed whether the c-Abl–SH2 domain could be recruited into FcRL1 microclusters after FcRL1 ligation. We expressed c-Abl–SH2-mCherry in CH27-HA-FcRL1-YFP cells and then stimulated them with PLBs containing either 30 nM F(ab′)2 anti-mouse MHC I or F(ab′)2 anti-HA for 10 min. TIRFM imaging illustrated that ligation of FcRL1, but not MHC I, efficiently induced c-Abl–SH2-mCherry recruitment into FcRL1 microclusters, suggesting that the cytoplasmic domain of FcRL1 can recruit the c-Abl–SH2 domain (Fig. 4, A and B). We did not use anti-IgM stimulation in this TIRFM imaging study since BCR engagement induce c-Abl recruitment into the tyrosine-phosphorylated ITAM of CD19 within the B cell immunological synapse as previously reported (*28*), and therefore, we could not discriminate the c-Abl–SH2-mCherry recruitment into FcRL1 or CD19.

BCR ligation induces phosphorylation of the Y_{281}ENV motif of FcRL1 to recruit c-Abl

To further verify whether c-Abl could interact with tyrosine-containing motifs within the FcRL1 cytoplasmic tail and identify the tyrosine-containing motif that was responsible for the interaction with the c-Abl–SH2 domain, we introduced mutations (Y281F, Y293F, and Y339F) in the three conserved tyrosine-based motifs (Y_{281}ENV, Y_{293}SLV, and Y_{339}EDA, respectively) within the cytoplasmic domain of the HA-FcRL1-YFP chimeric receptor. We transfected the WT and mutant chimeric receptors into CH27-FcRL1-KO cells and confirmed the expression levels of chimeric receptors on the cell surface to be similar (fig. S2C). We first cross-linked these cells by soluble F(ab′)2 fragment anti-HA (15 μg/ml) for 10 min before the subsequent coprecipitation with the purified glutathione *S*-transferase (GST) or c-Abl–SH2-GST fusion protein and immunoblotting with anti-YFP antibody (fig. S1J). Consistent with bioinformatics analysis results, only the Y281F mutant of the HA-FcRL1-YFP chimeric receptor lost its ability to associate with c-Abl–SH2-GST (Fig. 4C), whereas the WT and other two mutants of the HA-FcRL1-YFP chimeric receptor retained their binding affinity for the c-Abl–SH2 domain. Thus, the Y_{281}ENV motif within the cytoplasmic tail of FcRL1 most likely serves as the docking site for the SH2 domain of c-Abl.

To further validate the interaction between the pY_{281}ENV motif and the SH2 domain of c-Abl, we synthesized both phosphorylated and unphosphorylated peptides: biotin-GGA-STYPKSPDSRQPE PLY [*p] ENVNVVSGNEVYSLV and biotin-GGA-STYPKSPDSRQ-PEPLYENVNVVSGNEVYSLV. Enzyme-linked immunosorbent assay (ELISA) results indicated that only the pY_{281}ENV-containing peptide directly interacted with c-Abl–SH2-GST (Fig. 4D). To detect whether the tyrosine residue of the Y_{281}ENV motif could be phosphorylated after the ligation of FcRL1, we expressed the HA-FcRL1(WT)-YFP and HA-FcRL1(Y281F)-YFP chimeric receptors in CH27-FcRL1-KO cells, which were then stimulated with soluble F(ab′)2 fragment anti-HA (15 μg/ml) for 10 min. We tested the levels of tyrosine phosphorylation in these two types of chimeric receptors via immunoprecipitation with anti-HA antibodies and immunoblotting with the anti-phosphotyrosine 4G10 or anti-YFP antibodies. The WT and Y281F HA-FcRL1-YFP receptors were not phosphorylated in resting B cells. The ligation of FcRL1 induced tyrosine phosphorylation within the cytoplasmic tail of the HA-FcRL1(WT)-YFP receptor, which is consistent with published studies (*21*). The HA-FcRL1(Y281F)-YFP chimeric receptor only exhibited extremely weak phosphorylation upon FcRL1 ligation (Fig. 4E). These results indicated that ligation of the extracellular domain of FcRL1 mainly induced phosphorylation of the Y_{281}ENV motif in the cytoplasmic tail.

Next, it was important to address whether FcRL1 can function as the docking site of c-Abl when BCR is engaged with a specific antigen. As the ligation of BCR recruits FcRL1 into the B cell immunological synapse, we then investigated whether the Y_{281}ENV motif could be phosphorylated during the initiation of BCR signaling. To this aim, we stimulated CH27-FcRL1-KO B cells expressing either HA-FcRL1(WT)-YFP or HA-FcRL1(Y281F)-YFP chimeric receptors with soluble F(ab′)2 fragment anti-IgM (10 μg/ml) for 10 min. The extent of tyrosine phosphorylation upon BCR engagement was markedly lower in the mutant HA-FcRL1(Y281F)-YFP receptor than in the WT HA-FcRL1(WT)-YFP receptor as shown by immunoprecipitation and immunoblotting (Fig. 4E). Notably, unlike FcRL1 ligation, BCR ligation induced low-level tyrosine phosphorylation of the HA-FcRL1(Y281F)-YFP chimeric receptor (Fig. 4E), suggesting that BCR cross-linking may trigger the phosphorylation of other tyrosine residues including tyrosine residues in Y_{293}SLV and Y_{339}EDA motifs in addition to that in the Y_{281}ENV motif. These experiments illustrated that the pY_{281}ENV motif of FcRL1 could act as a docking site for the SH2 domain of c-Abl.

To demonstrate the recruitment of the whole c-Abl kinase into FcRL1 upon B cell activation, we performed TIRFM imaging experiment using the whole c-Abl kinase fused to mCherry. The c-Abl–mCherry was recruited into FcRL1 microclusters upon FcRL1 ligation, whereas the Y281F mutation in FcRL1 significantly reduced the recruitment of c-Abl into FcRL1 microclusters and the colocalization between FcRL1 and c-Abl (Fig. 4, F to I). For further immunoprecipitation experiments, we expressed c-Abl–mCherry-GST in CH27 B cells expressing HA-FcRL1(WT)-YFP or HA-FcRL1(Y281F)-YFP. The expression levels of c-Abl–mCherry-GST in these two types of cells were almost equal (fig. S2D). We stimulated both cell types with F(ab′)2 anti-mouse IgM (10 μg/ml) or F(ab′)2 anti-HA (15 μg/ml) for 10 min. Then, c-Abl fusion protein was coprecipitated with glutathione (GSH) beads and immunoblotted with anti-YFP antibody. The results showed that c-Abl was evidently associated with the HA-FcRL1(WT)-YFP chimeric receptor but not with the HA-FcRL1(Y281F)-YFP chimeric receptor upon ligation of BCR or FcRL1 (Fig. 4J). To further verify the recruitment of endogenous c-Abl to FcRL1, we stimulated CH27 B cells expressing either HA-FcRL1(WT)-YFP or HA-FcRL1(Y281F)-YFP with biotin-conjugated F(ab′)2 anti-HA antibodies (15 μg/ml) for 10 min. After cell lysis, HA-FcRL1(WT)-YFP or HA-FcRL1(Y281F)-YFP chimeric receptors bound to the biotinylated antibodies were precipitated by streptavidin beads and immunoblotted with anti–c-Abl antibodies, which indicated that the endogenous c-Abl was recruited to HA-FcRL1(WT)-YFP but not HA-FcRL1(Y281F)-YFP (Fig. 4K). Collectively, we concluded that the ligation of BCR induced tyrosine phosphorylation of the Y_{281}ENV motif of FcRL1 to recruit c-Abl for enhancement of B cell activation.

The mutation in the cytoplasmic Y_{281}ENV motif of FcRL1 impairs the BCR-mediated signaling and FcRL1-induced B cell proliferation

To further investigate the roles of the FcRL1 Y_{281}ENV motif and c-Abl signaling module in BCR signaling, we expressed HA-FcRL1(WT)-mCherry

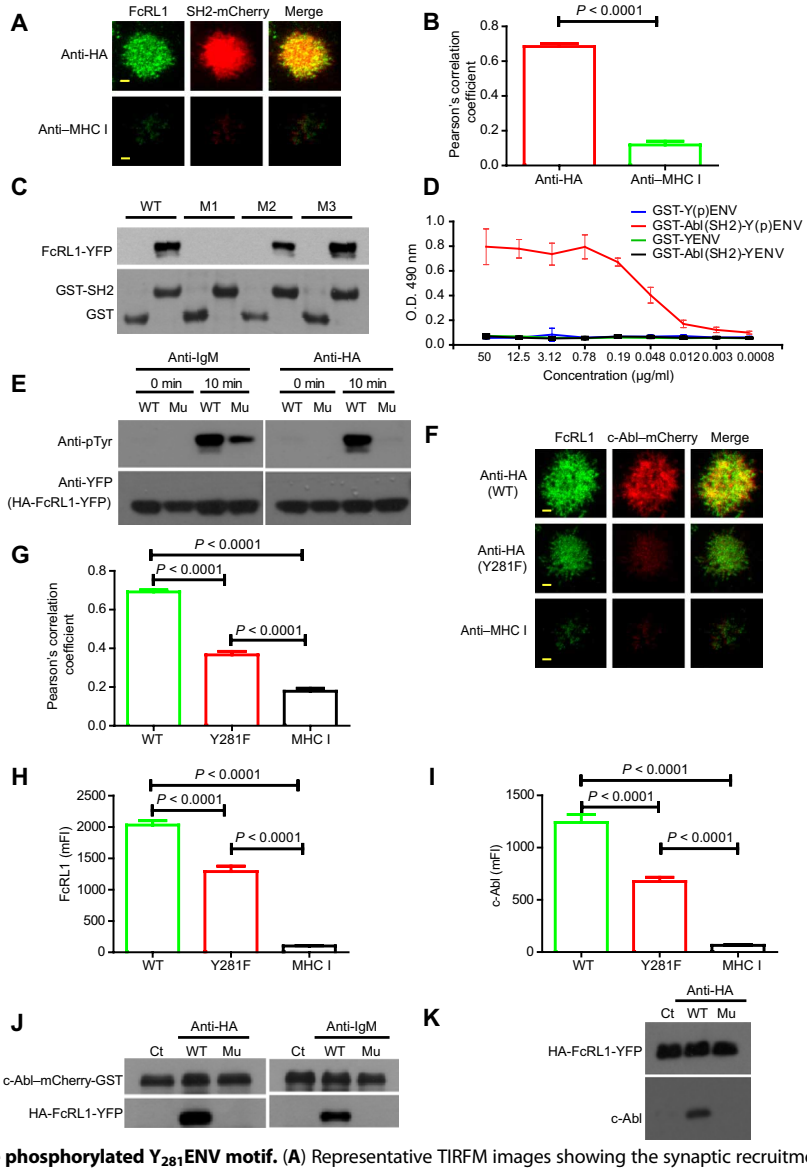

Fig. 4. FcRL1 recruits c-Abl via the phosphorylated Y_{281}ENV motif. (**A**) Representative TIRFM images showing the synaptic recruitment of the c-Abl–SH2 domain within FcRL1 clusters in CH27 cells stimulated via FcRL1 or MHC I ligation. Scale bars, 1.5 μm. (**B**) Colocalization analyses of the c-Abl–SH2 domain and FcRL1 microclusters in CH27 cells stimulated via FcRL1 or MHC I ligation ($n = 30$ cells). Experiments were repeated three times, and data from a representative experiment are shown. Bar represents means ± SEM. Two-tailed Student's *t* tests were used for statistical comparisons. (**C**) Detection of the interaction between the c-Abl–SH2 domain and FcRL1 via immunoprecipitation in CH27 cells stimulated via FcRL1 ligation. Immunoblots of glutathione *S*-transferase (GST) and GST-c-Abl–SH2 were probed with mouse anti-GST antibody. Immunoblots of FcRL1 chimeric receptors were probed with rabbit anti-YFP antibody. WT, HA-FcRL1(WT)-YFP; M1, HA-FcRL1(Y281F)-YFP; M2, HA-FcRL1(Y293F)-YFP; M3, HA-FcRL1(Y339F)-YFP. Experiments were repeated three times, and data from a representative experiment are shown. (**D**) Binding of different concentration of synthetic peptides of the FcRL1 intracellular domain to the c-Abl–SH2 domain as tested using ELISA. Binding was indicated by the optical density (O.D.) at 490 nm. Experiments were repeated three times, and data from a representative experiment are shown. Data are shown as means ± SD from triplicate replicates. (**E**) Tyrosine phosphorylation within HA-FcRL1(WT)-YFP and HA-FcRL1(Y281F)-YFP chimeric receptors expressed in CH27-FcRL1-KO cells stimulated via FcRL1 or BCR ligation. Immunoblots of phosphorylated tyrosine were probed with phosphorylated tyrosine-specific antibody 4G10. Immunoblots of FcRL1 chimeric receptors were probed with rabbit anti-YFP antibody. Mu, HA-FcRL1(Y281F)-YFP. Experiments were repeated three times, and data from a representative experiment are shown. (**F**) Given are representative TIRFM images showing the synaptic recruitment of the whole c-Abl kinase within FcRL1 clusters in CH27 B cells stimulated via FcRL1 or MHC I ligation. Scale bars, 1.5 μm. (**G**) Colocalization analyses of the whole c-Abl kinase and FcRL1 microclusters in CH27 B cells stimulated via FcRL1 or MHC I ligation. ($n = 40$ to 56 cells). Experiments were repeated three times, and data from a representative experiment are shown. Bar represents means ± SEM. Two-tailed Student's *t* tests were used for statistical comparisons. (**H** and **I**) Quantitative analysis of the mFI of FcRL1 microclusters (H) ($n = 42$ to 51 cells) and the c-Abl participated in FcRL1 microclusters (I) ($n = 37$ to 41 cells) in CH27 B cells stimulated via FcRL1 or MHC I ligation. Experiments were repeated three times, and data from a representative experiment are shown. Bar represents means ± SEM. Two-tailed Student's *t* tests were used for the statistical comparisons. (**J**) Detection of the interaction between the c-Abl–mCherry-GST and FcRL1 by immunoprecipitation in CH27 B cells stimulated via FcRL1 or BCR ligation. Immunoblots of c-Abl–mCherry-GST were probed with mouse anti-GST. Immunoblots of FcRL1 chimeric receptors were probed with rabbit anti-YFP antibody. Ct, control group without ligation. Experiments were repeated three times, and data from a representative experiment are shown. (**K**) Detection of the interaction between the endogenous c-Abl kinase and FcRL1 by immunoprecipitation in CH27 B cells stimulated via FcRL1 ligation. Immunoblots of endogenous c-Abl were probed with anti-c-Abl antibody. Immunoblots of FcRL1 chimeric receptors were probed with rabbit anti-YFP antibody. Experiments were repeated three times, and data from a representative experiment are shown.

or HA-FcRL1(Y281F)-mCherry in spleen primary B cells from FcRL1-KO mice. The cell surface expression levels of BCRs and FcRL1s were almost equal in these two types of B cells (fig. S2, E and F). TIRFM imaging and quantitative analysis demonstrated that the recruitment of BCR and the phosphorylated downstream kinases, including pSyk, pBLNK, and pPI3K (p85α), into the B cell immunological synapse was significantly lower in HA-FcRL1-Y281F–expressing primary B cells than in HA-FcRL1-WT–expressing primary B cells upon BCR engagement (Fig. 5, A to H).

The importance of tyrosine phosphorylation of the Y_{281}ENV motif within the cytoplasmic domain of FcRL1 could also be found in the proliferation in response to FcRL1 ligation. HA-FcRL1-Y281F–expressing primary B cells also exhibited a notably lower proliferative response to FcRL1 ligation than HA-FcRL1-WT–expressing primary B cells (Fig. 2D). To further confirm that the activity of FcRL1 in promoting proliferation was mediated through c-Abl, we inhibited the kinase activity of c-Abl using imatinib (*29*) before the ligation of FcRL1 and measured cell proliferation via CFSE dilution. The results indicated that c-Abl inhibition observably delayed proliferation induced by FcRL1 ligation (Fig. 2E). Collectively, these results verified that the promotion of proliferation by FcRL1 ligation was mediated through the recruitment of c-Abl to the pY_{281}ENV motif of FcRL1 and the kinase activity of c-Abl.

FcRL1 deficiency impaired both T cell–dependent and T cell–independent antibody responses

In contrast to the critical function of FcRL1 in BCR-mediated signaling, FcRL1 did not influence B cell development in FcRL1-KO mice, although the FcRL1 expression begins in the pre–B cell stage. Flow cytometric analyses revealed no obvious differences in the percentages of pro–B cells ($B220^+$ IgD^- IgM^- $CD43^+$), pre–B cells ($B220^+$ IgD^- IgM^- $CD43^-$), immature B cells ($B220^+$ IgD^- IgM^+ $CD43^-$), and mature B cells ($B220^+$ IgD^+) in the bone marrow between WT and FcRL1-KO mice. In addition, the percentages of transitional B cells ($B220^+$ $CD93^+$), follicular B cells ($B220^+$ $CD93^-$ $CD23^+$ $CD21^+$), and marginal zone B cells ($B220^+$ $CD93^-$ $CD23^-$ $CD21^{high}$) in the spleen were similar between the two mouse types (fig. S9, A to E). Thus, FcRL1 is dispensable for B cell development and homeostasis, suggesting that FcRL1 is probably not involved in tonic BCR signaling for B cell survival and development.

Next, we investigated whether FcRL1 deficiency influences antibody responses. To examine the function of FcRL1 in GC-mediated antibody responses, we immunized mice with sheep red blood cells on day 0 and quantified the formation of GCs in FcRL1-KO and WT control mice on day 7. Flow cytometric analyses demonstrated that the percentage of GC B cells among total B cells was distinctively reduced in FcRL1-KO mice compared with that in WT mice (Fig. 6, A and B). To further assess the T cell–dependent antibody response, we immunized both FcRL1-KO and WT control mice with a T cell–dependent model antigen NP32-KLH (4-hydroxy-3-nitrophenylacetyl-keyhole limpet hemocyanin) mixed with aluminum-containing adjuvant on day 0. FcRL1-KO mice produced notably lower amounts of NP-specific IgM and IgG antibodies than WT mice including NP-specific IgM (examined by NP8-BSA), high-affinity NP-specific IgG (examined by NP8-BSA), and total NP-specific IgG (examined by NP30-BSA) antibodies on days 7 and 14 after the primary immunization, as measured by ELISA (Fig. 6, C to E). Moreover, we performed enzyme-linked immunosorbent spot experiments to quantify the antibody-forming cells producing NP-specific IgM or IgG antibodies in these two types of mice on days 3 and 6 to examine the effect of FcRL1 deficiency on extrafollicular plasmablast response. The results consistently demonstrated that FcRL1 deficiency reduced the number of antigen-specific extrafollicular plasmablasts (Fig. 6, F to H).

Last, to examine the function of FcRL1 in T cell–independent antibody responses, we immunized both FcRL1-KO and WT mice with the T cell–independent model antigen NP50-Ficoll mixed with aluminum-containing adjuvant on day 0. We performed ELISA experiments to quantify the NP-specific IgM and IgG_3 (examined by NP30-BSA) on days 0 and 7, respectively. The results suggested that FcRL1 deficiency also significantly affected T cell–independent antibody responses (Fig. 6, I and J). Collectively, these data suggest that although FcRL1 is dispensable for B cell development and homeostasis, FcRL1 plays an important role in the promotion of both T cell–dependent and T cell–independent antibody responses.

DISCUSSION

BCR signaling is subject to strict regulation by both activating co-receptors, including CD19, and inhibitory co-receptors, including FcγRIIB. The discovery of the large family of FcRL molecules has considerably broadened the view of complicated functions of B cell co-receptors (*20*). Unlike most FcRL family members, which usually play a negative regulatory role on B cell activation, FcRL1, in contrast, positively regulates the initiation of B cell activation. Sequences of the conservative tyrosine-based motifs in the FcRL1 cytoplasmic tail, namely, G-S-T-Y-P-K-S-X9-Y-E-N-V, X8-Y-S-L-V and G-L-Y-S-K-X9-Y-E-D-A, differ from the canonical ITAM sequence D/E-X-XY-X-X-L/I-X-8-Y-X-X-L/I in the BCR subunits CD79A and CD79B (*30*), which recruit Syk, BTK, BLNK, and PLC-γ2 upon antigen binding. Our results demonstrated that the positive role of FcRL1 is based on the recruitment of c-Abl through the phosphorylated Y_{281}ENV motif in its cytoplasmic tail. FcRL1 was recruited into the B cell immunological synapse together with BCRs upon the ligation of BCRs alone, and the subsequent phosphorylation of tyrosine residues in the Y281ENV motif within the intracellular of FcRL1 provided an ideal docking site for the SH2 domain–containing kinase c-Abl. In turn, the FcRL1 and c-Abl signaling module potently augmented B cell activation and proliferation. Despite its BCR signal-enhancing function, FcRL1 deficiency did not affect B cell development and homeostasis. However, FcRL1 was important for both T cell–dependent and T cell–independent antibody responses because FcRL1 deficiency markedly impaired the formation of extrafollicular plasmablasts and/or GCs with notably decreased antibody production in response to T cell–dependent or T cell–independent antigens.

Mechanistically, FcRL1 shares some common features with the well-characterized BCR-activating co-receptor CD19 in B cell activation and function. First, both FcRL1 and CD19 can be passively recruited into the B cell immunological synapse by BCR cross-linking alone, and upon their respective synaptic recruitment, both receptors can recruit c-Abl through the SH2 domain–phosphotyrosine interaction (*22*, *28*). Second, both FcRL1 and CD19 function through the intracellular tyrosine-containing motif. In this study, we observed that FcRL1 deficiency or mutations in the Y_{281}ENV motif markedly impaired BCR signaling and humoral antibody responses. In the literature, mutations of Y482 and Y513 in the respective YDEM and YENM motifs within the cytoplasmic domain of CD19, which are binding sites of the p85α unit of PI3K, impaired the function of

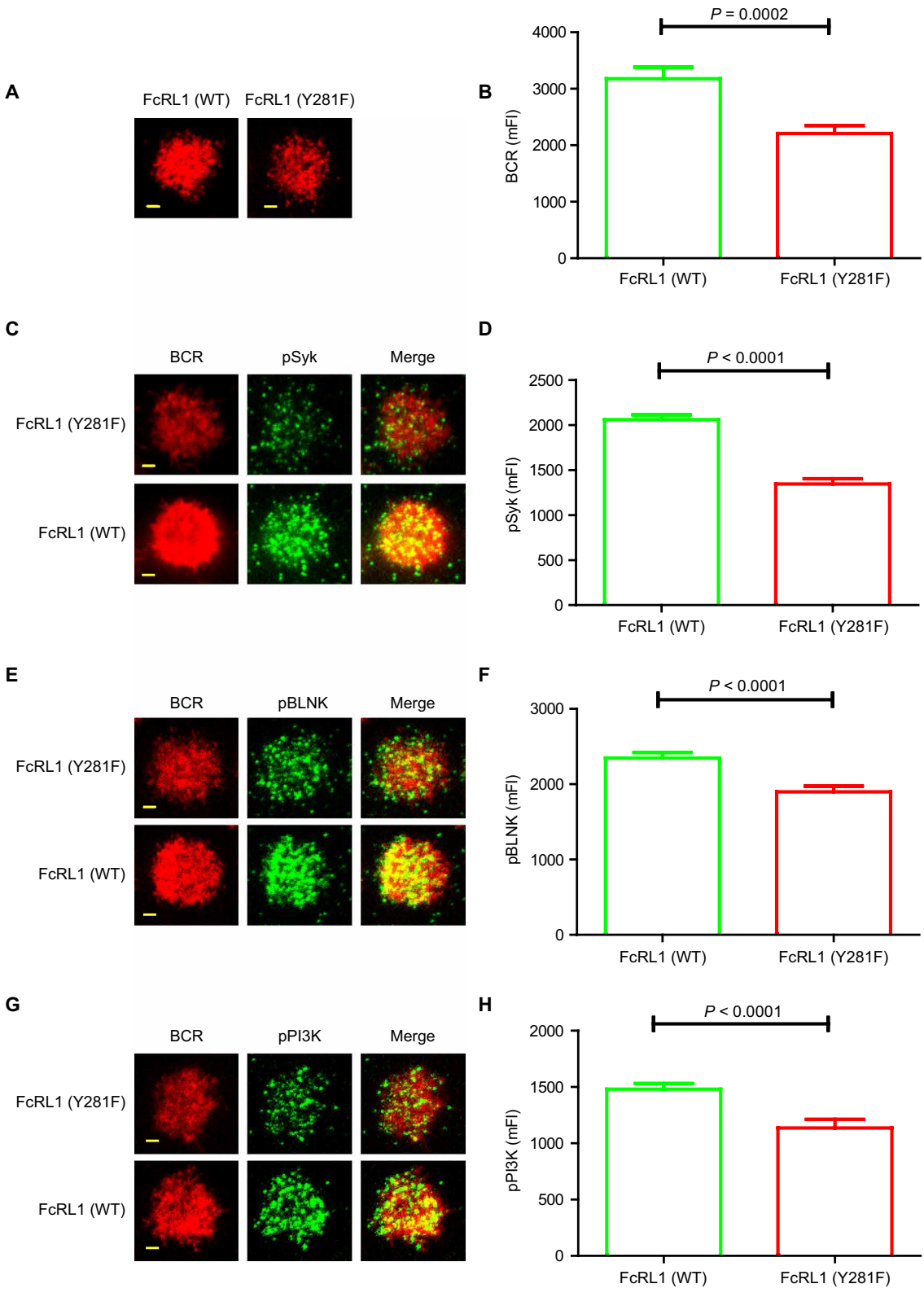

Fig. 5. Mutation of Y_{281}ENV motif in FcRL1 impairs BCR engagement–induced B cell activation in the absence of FcRL1 ligation. Left: Representative TIRFM images showing the synaptic recruitment of BCRs (**A**), pSyk (**C**), pBLNK (**E**), and pPI3K (p85α) (**G**) in FcRL1-KO primary B cells expressing HA-FcRL1(WT)-YFP and HA-FcRL1(Y281F)-YFP chimeric receptors. Scale bars, 1.5 μm. Right: Quantitative analysis of the mFI of synaptic BCRs (**B**) ($n = 34$ to 36 cells), pSyk (**D**) ($n = 72$ to 77 cells), pBLNK (**F**) ($n = 76$ to 96 cells), and pPI3K (p85α) (**H**) ($n = 60$ to 75 cells). Experiments were repeated three times, and data from a representative experiment are shown. Bar represents means ± SEM. Two-tailed Student's *t* tests were used for the statistical comparisons.

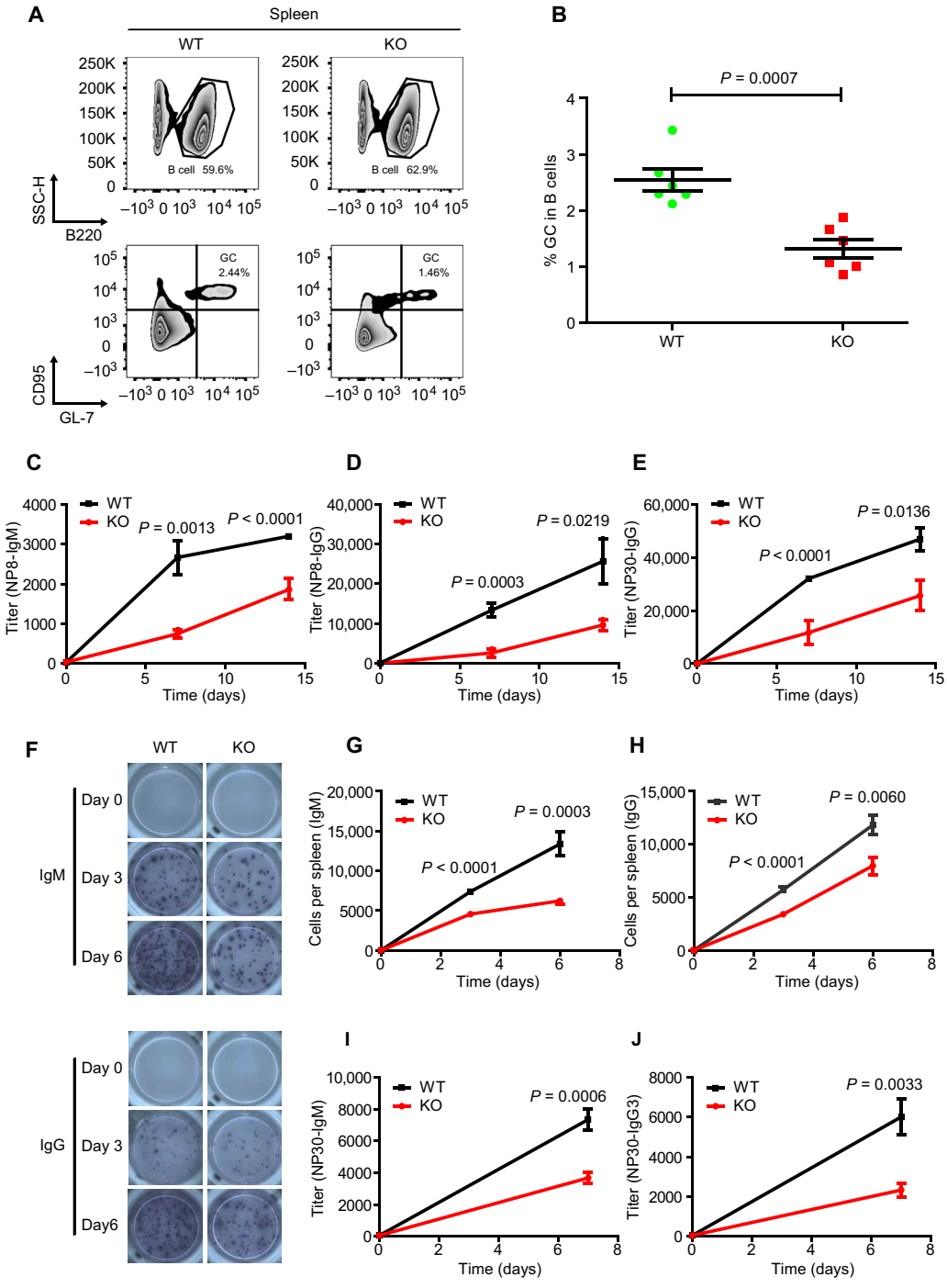

Fig. 6. FcRL1 deficiency impairs the germinal center formation and antibody responses. (**A** and **B**) Representative flow cytometric gating (A) and quantitative analysis of the percentage of GC B cells (B) in the spleens of FcRL1-KO and WT mice ($n = 6$ mice per group) immunized with sheep red blood cells for 7 days. Each symbol represents one mouse. Experiments were repeated three times, and data from a representative experiment are shown. Bar represents means ± SD. Two-tailed Student's *t* tests were used for statistical comparisons. SSC-H, side scatter–height. (**C** to **E**) Antibody titers from FcRL1-KO and WT mice ($n = 6$ mice per group) at different times after immunization with 5 μg of NP32-KLH and Imject Alum Adjuvant. Sequential serum ELISA was performed to detect NP-specific antibody. NP8-BSA for IgM (C), NP8-BSA for IgG (D), and NP30-BSA for IgG (E) were used as the coating antigens. Experiments were repeated three times, and data from a representative experiment are shown. Bar represents means ± SEM. Two-tailed Student's *t* tests were used for statistical comparisons. (**F** to **H**) Representative enzyme-linked immunosorbent spot assays (F) and quantitative analysis of NP-specific IgM (G) and IgG antibody-forming cells (H) in the spleens of FcRL1-KO and WT mice ($n = 9$ mice per group). Experiments were repeated three times, and data from a representative experiment are shown. Bar represents means ± SEM. Two-tailed Student's *t* tests were used for statistical comparisons. (**I** and **J**) Antibody titers from FcRL1-KO and WT mice ($n = 6$ mice per group) at different times after immunization with 20 μg of NP50-Ficoll and Imject Alum Adjuvant. Sequential serum ELISA was performed to detect the NP-specific antibody. NP30-BSA for IgM (I) and NP30-BSA for IgG_3 (J) were used as the coating antigens. Experiments were repeated three times, and data from a representative experiment are shown. Bar represents means ± SEM. Two-tailed Student's *t* tests were used for statistical comparisons.

CD19 as a booster for B cell activation and function (*31*, *32*). Physiologically, our works provide sufficient evidence that FcRL1 plays a positive regulatory role in B cell proliferation and T cell–dependent and T cell–independent antibody responses. These phenotypes are largely comparable with observations in CD19-KO mice or CD19 Y482/Y513 mutation mice (*31*, *33*, *34*).

Nonetheless, there are marked differences between the functions of CD19 and FcRL1 in B activation and function. First, the ligation of CD19 alone could trigger intracellular Ca^{2+} flux because CD19 associates with CD21, CD81, and Leu^{13} to form a signal transduction complex that is independent of the BCR complex (*35*, *36*). In contrast, FcRL1 cross-linking alone could not trigger Ca^{2+} flux (*21*, *37*), but to date, it is not known whether a native FcRL1 ligand exists or FcRL1 associates with a so far unknown ligand-binding receptor. FcRL1 does not bind to the Fc portion of any Ig isotype (IgM, IgA, IgG_1, IgG_2, IgG_3, and IgG_4), although it shares the same ancestor as FcRs (*21*). Analyses of amino acid sequences of the transmembrane domain of FcRL1 uncovered the presence of multiple polar amino acid residues, such as serine and threonine, which could mediate FcRL1 to interact with other membrane receptors through the formation of a dynamic signal transduction complex in the transmembrane region.

Second, FcRL1 deficiency does not impair B cell development, which is also a distinct finding from published studies, showing that CD19 notably contributes to B cell development in the bone marrow (*38*). Moreover, it has also been reported that marginal zone B cells are absent in CD19-KO 129Sv/J mice and the differentiation and/or survival of B1 cells and marginal zone B cells is dependent on CD19 Y482 and/or Y513 (*31*). Although both CD19 and FcRL1 share c-Abl as the same downstream signaling molecule, we believe that their interaction mechanisms are fundamentally different. CD19 and c-Abl are believed to undergo constitutive interaction in resting B cells independent of BCR cross-linking (*33*). Moreover, in vitro phosphorylation assays demonstrated that CD19 is the substrate of c-Abl because c-Abl could directly phosphorylate the cytoplasmic domain of CD19 encompassing amino acids 362 to 540, which is the region for the recruitment of Vav and PLC-γ2, Fyn and/or Lyn, and PI3K (*31*). As a nonreceptor tyrosine kinase, c-Abl is involved in both the regulation of cytoskeletal remodeling and cell proliferation and V(D)J recombination during B cell development (*39*). Therefore, the absence of CD19 may impair the function of c-Abl in the integrity of tonic BCR signaling. These studies may explain why CD19 deficiency impairs B cell development. Findings of the present study demonstrated that FcRL1 phosphorylation in resting B cells is extremely rare and, consequently, there is no constitutive interaction between FcRL1 and c-Abl. c-Abl recruitment and its interaction with c-Abl occur only when the Y_{281}ENV motif is phosphorylated in response to antigen stimulation. Thus, it is not unexpected that FcRL1 is not essential for B cell development and survival.

In addition, the phosphorylation states of tyrosine residues in FcRL1 induced by FcRL1 or BCR ligation are different, indicating that the kinases involved in FcRL1 phosphorylation under these two stimulation conditions may be different. Although these kinases have not been identified, the function of the FcRL1–c-Abl signal module in enhancing B cell activation and proliferation was defined in this study. FcRL1 transcription levels are high in naïve B cells and notably lower in pre-GC, GC, and plasma cells (*21*). We provided evidence that the absence of FcRL1 reduced B cell proliferation and T cell–dependent and T cell–independent antibody responses.

In our report, to further verify that FcRL1 recruits c-Abl via the phosphorylated Y_{281}ENV motif, we fused HA tag at the extracellular domain of FcRL1 and cross-link FcRL1 by anti-HA antibody to promote FcRL1 oligomerization. Specific anti-mouse FcRL1 antibody is required for further study of the biological function of FcRL1 in future studies. Moreover, since FcRL5 is primarily expressed by marginal zone B cells and B-1 B cells, future studies shall use these two types of subset B cells for the quantification of FcRL5 at both transcription and protein level.

In summary, these results illustrate the critical and entirely previously unidentified role of FcRL1 that enhances B cell activation and function in response to BCR stimulation alone in a B cell–intrinsic manner through its recruitment to B cell immunological synapses and subsequent recruitment of c-Abl.

MATERIALS AND METHODS

Mice

C57BL/6 (JAX664) mice were purchased from the Jackson Laboratory. FcRL1-KO mice were generated by CRISPR-Cas9 technique in C57BL/6 background and were then backcrossed with WT C57BL/6 for at least three generations before further functional experiments. Mice were maintained under specific pathogen–free conditions. Mouse experiments were performed according to the Institutional Animal Care and Use Committee (#F16-00228-A5916-01 to Tsinghua University) and Institutional Review Board (#15-LWL2 to Liu Lab) and guidelines for animal welfare.

Cells and plasmids

The CH27 cell line was purchased from American Type Culture Collection and maintained in complete RPMI 1640 with 10% heat-inactivated fetal bovine serum (FBS) and antibiotics. Primary B cells from the mouse spleen were purified using a MACS B cell negative isolation kit (Miltenyi Biotec), frozen in 10% dimethyl sulfoxide, and kept in liquid nitrogen until usage. The coding frames of full-length FcRL1 (Q8R4Y0, UniProt), full-length FcRL5 (Q68SN8-1, UniProt), full-length FcγRIIB (P08101-1, UniProt), full-length c-Abl (P00520, UniProt), and the c-Abl–SH2 domain (amino acids 127 to 217) were amplified from a mouse spleen complementary DNA (cDNA) library. The expression plasmids for HA-FcRL1(WT)-YFP/mCherry, c-Abl–SH2-mCherry, c-Abl–mCherry, FcRL5-YFP, and FcγRIIB-YFP were constructed into the pHAGE backbone by Gibson assembly. The HA-FcRL1(Y281F)-YFP/mCherry, HA-FcRL1(Y293F)-YFP, and HA-FcRL1(Y339F)-YFP mutant plasmids were constructed via mutation PCR based on HA-FcRL1(WT)-YFP/mCherry. The CH27-HA-FcRL1(WT)-YFP/mCherry, CH27-HA-FcRL1(Y281F)-YFP, CH27-HA-FcRL1(Y293F)-YFP, and CH27-HA-FcRL1(Y339F)-YFP cell lines were constructed via lentiviral transduction of the corresponding plasmids into FcRL1-KO CH27 cells and fluorescence-activated cell sorting. HA-FcRL1(WT)-mCherry and HA-FcRL1(Y281F)-mCherry were constructed into the pMSCV (Murine Stem Cell Virus plasmid) backbone for the subsequent lentiviral transduction into primary B cells from FcRL1-KO mouse.

Peptides and antibodies

The biotin-GGAGGA-STYPKSPDSRQPEPLY [*p] ENVNVVSGNEVYSLV and biotin-GGAGGA-.STYPKSPDSRQPEPLYENVNVVSGNEVYSLV peptides were synthesized and purified via

high-performance liquid chromatography, and >90% purity was verified using mass spectrometry. All the whole antibodies (full IgG) that were used in our experiments are commercially available: donkey IgG anti-mouse IgM, μ chain–specific (715-065-140, Jackson ImmunoResearch Laboratory), rat IgG anti-mouse MHC I (MCA2398, AbD Serotec), and mouse IgG anti-HA (B1168, BioDragon). F(ab′)2 or Fab fragments of these antibodies were acquired by digesting whole IgG antibodies using a commercially available kit following the manufacturer's protocols: Pierce F(ab′)2 Preparation Kit (#44988) and Pierce Fab Preparation Kit (#44685). The antibodies were conjugated to biotin using Biotin Protein Labeling Kit (#11418165001, Sigma-Aldrich). Alexa Fluor 647 AffiniPure Fab fragment goat anti-mouse IgM, μ chain–specific (115-607-020, Jackson ImmunoResearch Laboratory) was used to label IgM-BCRs. Fab fragment anti-HA antibodies were conjugated to Alexa Fluor 647 dye using Alexa Fluor monoclonal antibody labeling kits (Invitrogen). 4G10 (#05-1050, Platinum) was used to immunoblot the phosphorylated tyrosine of FcRL1. Rabbit polyclonal anti-YFP antibody (B1025F, BioDragon) was used for immunoblotting of the YFP fusion protein. The c-Abl antibody (2862, Cell Signaling Technology) was used for the immunoblot of endogenous c-Abl.

Molecular imaging using TIRFM

PLBs containing biotinylated anti-mouse Ig surrogate antigen were prepared following our published protocols (*40*). B cells were first stained with Alexa Fluor 647 AffiniPure Fab fragment goat anti-mouse IgM, μ chain–specific (115-607-020, Jackson ImmunoResearch Laboratory) and then loaded on the chamber to react with surrogate antigens on the PLBs for at least 10 min, followed by 4% paraformaldehyde (PFA) fixation. TIRFM images were captured using an Olympus IX-81 microscope supported by an Andor iXon$^+$ DU-897D electron-multiplying charge-coupled device camera, Olympus 100 × 1.49 numerical aperture objective lens, and TIRF port. TIRFM image acquisition was controlled by MetaMorph software (Molecular Devices), and the exposure time for 512 × 512 pixel images was 100 ms. The mFIs of BCR, FcRL1, and intracellular signaling molecules accumulated at the immunological synapse were statistically analyzed according to the intensity and area using ImageJ software [National Institutes of Health (NIH)].

Intracellular immunofluorescence staining

Intracellular immunofluorescence staining of the intracellular signaling molecules in the immunological synapse of activated B cells was performed according to our published protocols (*41*). Briefly, B cells were fixed with 4% PFA for 30 min at room temperature. After washing with 1× phosphate-buffered saline (PBS), B cells were permeabilized with 0.2% Triton X-100 for 20 min and then blocked with goat nonspecific IgG (100 μg/ml; 005-000-003, Jackson ImmunoResearch Laboratory) for 1 hour at room temperature. Subsequently, cells were incubated with various primary antibodies including anti–phospho-Syk (pY525/526) antibody (1:500 dilution; #2711, Cell Signaling Technology), anti–phospho-PI3K p85 (pY458)/p55 (pY199) antibody (1:500 dilution; #4228, Cell Signaling Technology), and anti–phospho-BLNK antibody (1:500 dilution; BioDragon) at 37°C for 1 hour, followed by Alexa Fluor 568–conjugated F(ab′)2 fragment goat anti-rabbit IgG (1:2000 dilution; A21069, Invitrogen) as the secondary antibody. TIRFM images were analyzed using ImageJ (NIH).

Real-time PCR

Total RNA from either CH27 or primary B cells was extracted using the HiPure Total RNA Mini Kit (R4111, Magen). Total cellular RNA was primed with oligo(dT) primers and was reverse-transcribed with RevertAid First Strand cDNA Synthesis Kit (K1622, Thermo Fisher Scientific) into single-stranded cDNA. Gene-specific primers for real-time PCR were as follows: moFcRL1, 5′-CACACGGAGTAAGTGAGTCCT-3′ (forward) and 5′-TCAGGCCTTGGGCTTGTATG-3′ (reverse); moFcRL5, 5′-GCCAAGCCGACAGCTTACTTC-3′ (forward) and 5′-ACAGCAGGTGGAGCTTGCA-3′ (reverse); glyceraldehyde-3-phosphate dehydrogenase, 5′-GGTGAAGGTCGGTGTGAACG-3′ (forward) and 5′-CTCGCTCCTGGAAGATGGTG-3′ (reverse). Briefly, the cDNA of CH27-WT or CH27-FcRL1-KO cells set three parallel repeats, respectively. Six FcRL1-KO mice and six FcRL1-WT control mice were prepared for total RNA extraction. The cDNA templates of every two mice in the same group were mixed into one sample. The real-time PCRs were performed following the manufacturer's instructions with 2× RealStar Power SYBR Mixture (A311-101, GenStar) and run on CFX Connect Real-Time System (Bio-Rad). Each amplification reaction underwent initial denaturation at 95°C for 3 min, followed by 40 cycles of denaturation at 95°C for 10 s and annealing at 60°C for 45 s.

B cell proliferation analysis

Primary B cells from mouse spleens were stained with 1 μM CFSE (Invitrogen) at 37°C for 10 min and then seeded in 24-well plates in 500 μl of medium containing 50 μM β-mercaptoethanol, rm–interleukin-4 (20 ng/ml), and F(ab′)2 fragment anti-mouse IgM (10 μg/ml) or F(ab′)2 fragment anti-HA (15 μg/ml) to ligate BCRs or FcRL1s (*42*). PBS was used in place of F(ab′)2 fragment anti-mouse IgM or F(ab′)2 fragment anti-HA as a control. After stimulation for 72 hours, the CFSE fluorescence intensity was measured using flow cytometry, and data were analyzed using FlowJo software (Tree Star). Mathematical analysis of the CFSE dilution was performed using gates for divided/undivided cells to assess the percentage of increased/decreased proliferation. Regarding the inhibition of c-Abl kinase activity, primary B cells were incubated with 50 nM imatinib-containing medium (*29*) during the whole process of proliferation testing.

Enzyme-linked immunosorbent assay

We measured the capacity of the c-Abl–SH2 domain to bind to synthetic peptides using ELISA. Briefly, synthetic peptides (50 μg/ml) (biotin-GGA-STYPKSPDSRQPEPLY [*p] ENVNVVSGNEVYSLV and biotin-GGA-STYPKSPDSRQPEPLYENVNVVSGNEVYSLV) were diluted fourfold in PBS buffer to create a concentration gradient and coated onto Nunc MaxiSorp ELISA plates overnight at 4°C. The plates were further blocked with 0.3% (w/v) gelatin in PBS buffer for 2 hours at 37°C, followed by the addition of GST (10 μg/ml) or GST-SH2 fusion proteins for 1 hour at 37°C. The plates were then washed with PBST buffer (PBS with 0.05% Tween 20) and incubated with mouse anti-GST antibody (clone N100/13, NeuroMab) for 1 hour at room temperature. After washing, plates were incubated with horseradish peroxidase (HRP)–conjugated goat anti-mouse Ig (00090941, Dako) as the second antibody for 45 min at room temperature. After washing, the substrate solution, comprising 0.325% *o*-phenylenediamine dihydrochloride (Sigma-Aldrich) and 0.085% H_2O_2 in 0.3 M tris-citrate buffer (pH 6.0), was added. After incubation at room temperature for 10 min in the dark, the reaction was stopped with 2.5 M H_2SO4, and the plates were measured using an ELISA plate reader (Bio-Rad) for light absorbance at 490 nm.

Enzyme-linked immunosorbent spot

For the extrafollicular plasmablast numbers test, mice were injected intraperitoneally with 5 μg of NP32-KLH and Imject Alum Adjuvant on day 0. Splenic cells were collected on days 0, 3, and 6. Polyvinylidene difluoride 96-well plates were coated with NP30-BSA (5 μg/ml). Plates were further blocked with 10% FBS in RPMI 1640, followed by seeding the splenic single cells at a dilution of approximately 2×10^5 per well. After incubation for 16 hours, cells were washed with PBST buffer. The plates were then incubated with biotin-conjugated rat anti-mouse IgM (#553406, BD Biosciences) or biotin-conjugated goat anti-mouse IgG (H+L) (SAB4600004, Sigma-Aldrich) for 1 hour at room temperature. After washing, the plates were incubated with streptavidin–alkaline phosphatase (S921, Invitrogen). BCIP/NBT (5-bromo-4-chloro-3-indolyl phosphate/nitro blue tetrazolium) (TA-500-ABS, Thermo Fisher Scientific) served as the substrate of alkaline phosphatase.

Ca^{2+} mobilization analysis

To detect intracellular Ca^{2+} mobilization in B cells, cells were processed with Fluo-4 AM (acetoxymethyl ester) (2 μg/ml; Invitrogen) and Fura Red AM (3 μg/ml; Invitrogen) at 30°C for 20 min using 2.5 mM probenecid (Invitrogen) in Hanks' balanced salt solution (HBSS) buffer (with 1.26 mM Ca^{2+}) with 1% FBS. Then, cells were washed with HBSS once and incubated at 37°C for 20 min in HBSS buffer (with 1.26 mM Ca^{2+}) containing 1% FBS. After the basal Ca^{2+} concentration was monitored for 50 s, cells were stimulated with different antigens. CH27 cells were stimulated with PC_{10}-BSA (15 μg/ml). Primary B cells were stimulated with F(ab′)2 fragment anti-mouse IgM (10 μg/ml). Fluo-4 and Fura Red fluorescence was measured using a BD Accuri C6 or LSR II cytometer. The Fluo-4–to–Fura Red ratio was calculated using FlowJo (Tree Star) and normalized on the basis of its basal level.

Protein expression and purification

The coding frame of the c-Abl–SH2 domain (amino acids 127 to 217) was amplified from mouse cDNA library and inserted into the pGEX-6P-1 vector. The GST tag and c-Abl–SH2-GST fusion protein were expressed in the BL21 vector (DE3) and purified using GST beads. The protein purity was examined by SDS–polyacrylamide gel electrophoresis.

Gene deletion using CRISPR-Cas9 system

The sgRNA (5′-CTCTATCAACCGAGCAGATG-3′) applied to delete the FcRL1 gene from CH27 cells was designed online (http://crispr.mit.edu/) and inserted into the pSpCas9-2a-YFP vector. The pSpCas9-2a-YFP vector carrying specific sgRNA was transiently transfected into CH27 cells by Amaxa Nucleofector II Device (Lonza). After a culturing time of 16 hours, YFP-positive CH27 cells (usually 10 to 20%) were sorted by flow cytometry and subcloned in 96-well plates. Genomic DNA of each individual cell clone was extracted using TIANamp Genomic DNA Kit (R6802). The mutation was verified by PCR and Sanger sequencing (forward, 5′-GGATGGGAGATGACATCACATTCTCTACGG-3′; reverse, 5′-ATCTGTGTTACTTACCTCTGACGTGGATGCTCACC-3′). The KO efficiency was confirmed at the protein level by Western blotting using a specific anti-FcRL1 antibody (11536-RP02, Sino Biological).

FcRL1-KO mice were generated using the CRISPR-Cas9 tool. Two sgRNAs (5′-GGGTGCTGAACTGTTCCCC-3′ and 5′-GGCTTAGAATAGAGTCCAG-3′) targeting the 4th and 10th exons were designed online (http://crispr.mit.edu/), and the T7 promoter was added to the 5′ end of sgRNA via PCR. A MEGAshortscript High Yield Transcription Kit was used for the in vitro transcription of sgRNA. The Cas9-encoding gene was inserted into the pST1374-N-NLS-flag-linker-Cas9 vector with the T7 promoter as a template, and mMESSAGE mMACHINE T7 Ultra Kits were used for the in vitro transcription of Cas9 mRNA. Both the sgRNA and Cas9 mRNA transcription products were purified using a MEGAclear kit, mixed together to final concentrations of 50 ng/μl (sgRNA) or 100 ng/μl (Cas9 mRNA), and simultaneously delivered into zygotes from C57BL/6 mice via microinjection. Then, zygotes were transplanted into recipient mice, and the FcRL1-KO offspring were backcrossed with WT C57BL/6 mice for at least three generations. The FcRL1-KO homozygote genotype was confirmed at the genome level using PCR. The primers used for PCR were as follows: WT, 5′-AGTGAGCTGGTGAGCATCCACGTCAGAG-3′ (forward) and 5′-AAGTTGAGAGCCACCACCTCACTTCGTTGGGC-3′ (reverse); KO, 5′-TGATGGAGGGAGACAAGCTGGTCCTCAT-3′ (forward) and 5′-TTCCTGGGTGGTTTCTGCAGGACTTGC-3′ (reverse). The PCR products were resolved via agarose gel electrophoresis. The FcRL1-KO homozygote genotype exhibited an 800–base pair (bp) product, whereas the FcRL1 WT genotype produced a 500-bp product. The KO efficiency at the protein level was confirmed via Western blotting using a specific anti-FcRL1 antibody (11536-RP02, Sino Biological).

For the verification of the specificity of the anti-FcRL1 antibody (11536-RP02, Sino Biological), the pHAGE-FcRL1/FcRL5/FcγRIIB-YFP plasmids were transiently transfected into 293F cells for 24 hours. Western blot was performed to verify the specificity of anti-FcRL1 antibody (11536-RP02, Sino Biological), with rabbit polyclonal anti-YFP antibody as a control for expression (B1025F, BioDragon).

Off-target detection

The potential off-targets of the sgRNA were analyzed online (http://crispr.mit.edu/). The top 3 potential off-target gene loci with high scores were amplified using PCR and sequenced to detect mutations.

Retroviral infection of mouse primary splenic B cells

Mouse primary splenocytes were isolated from C57BL/6 mice. After 24 hours of incubation with lipopolysaccharide (10 μg/ml; Sigma-Aldrich) in RPMI 1640 containing 10% FBS, penicillin, streptomycin, and 50 μM β-mercaptoethanol, 4×10^6 splenic cells were spin-infected for 3.5 hours with 1.5 ml of concentrated retrovirus supernatants from Plat-E cells transfected with pMSCV expression vectors encoding HA-FcRL1(WT)-mCherry or HA-FcRL1(Y281F)-mCherry. At 24 hours after retroviral infection, the positive rate was measured using flow cytometry, and the infection efficiency usually reached 30 to 50%.

Immunoprecipitation and immunoblotting

Immunoprecipitation and immunoblotting were performed as described previously. CH27-HA-FcRL1-YFP cells (1×10^7 cells/ml) were preincubated with serum-free RPMI 1640 at 37°C for 30 min (starvation) and resuspended at 5×10^7 cells/ml in fresh serum-free medium. Cells were stimulated with F(ab′)2 fragment anti-mouse IgM (10 μg/ml) or biotin-conjugated F(ab′)2 fragment anti-HA (15 μg/ml) at 37°C. Cells were lysed with 1% Triton X-100 lysis buffer. For the immunoprecipitation assay with GSH beads, cell lysates were precleared with GSH beads link-coupled with GST protein for

2 hours. Then, the lysed cells were immunoprecipitated with GSH beads link-coupled with GST or GST-SH2 at 4°C for 6 hours. During the detection of the interaction between c-Abl–mCherry-GST and FcRL1, the precleared step was omitted. To quantify the immunoprecipitated proteins, immunoblots were probed with rabbit anti-YFP antibody. For the immunoprecipitation assay with anti-HA, the HA-FcRL1-YFP chimeric receptors were captured by biotin-conjugated F(ab′)2 fragments anti-HA and then precipitated by beads conjugated with streptavidin.

Flow cytometry

Single-cell leukocyte suspensions from the bone marrow and spleen were used in the flow cytometry experiments. CD16/CD32 (93, BioLegend) was used to block FcRs. The following antibodies [conjugated to eFluor 450, fluorescein isothiocyanate, phycoerythrin (PE), PE-Cy5, PerCP/Cy5.5, and PE-Cy7] were used: anti-CD21 (7G6, BD Biosciences), anti-CD23 (B3B4, eBioscience), anti-CD43 (S7, BD Biosciences), anti-CD93 (AA4.1, eBioscience), anti-CD95 (15A7, eBioscience), anti-B220 (RA3-6B2, BD Biosciences), anti-GL7 (GL-7, eBioscience), anti-IgD (11-26c.2a, BD Biosciences), and anti-IgM (II/41, eBioscience). Detection of cell surface marker expression was performed using an LSRFortessa cytometer (BD Biosciences). Typically, living lymphocytes, judged by forward and side scatter parameters, were gated for analysis. Data were further analyzed using FlowJo (Tree Star).

Flow cytometry sorting

HA-FcRL1(WT/mutant)-YFP/mCherry or BCR expressed on the surface of CH27 cells or primary B cells was stained with Alexa Fluor 647–conjugated Fab anti-HA (100 nM) or Alexa Fluor 647–conjugated Fab anti-IgM (100 nM). Cells with similar expression level were sorted out with a FACSAria (BD Biosciences).

Immunization and serum analysis

Concerning T cell–dependent immune responses, mice were injected intraperitoneally with 5 μg of NP32-KLH and Imject Alum Adjuvant on day 0. Sera were collected on days 0, 7, and 14. Regarding T cell–independent immune responses, mice were injected intraperitoneally with 20 μg of NP50-Ficoll. Sera were collected on days 0 and 7. The levels of Ag-specific antibodies of different isotypes were determined by ELISA using 96-well plates coated with NP-BSA (NP8-BSA or NP30-BSA). The plates were further blocked with 0.3% gelatin in PBS buffer for 2 hours at 37°C, followed by the incubation of serially diluted serum at 37°C for 1 hour. HRP-conjugated goat anti-mouse IgM (#1021-05, SouthernBiotech), HRP-conjugated goat anti-mouse IgG Fc (#1033-05, SouthernBiotech), or HRP-conjugated goat anti-mouse IgG3 (#115-035-209, Jackson ImmunoResearch Laboratory) was diluted 1:10,000 to detect the antibody. The substrate reaction and data analysis were performed as described previously in ELISA.

SUPPLEMENTARY MATERIALS

Supplementary material for this article is available at http://advances.sciencemag.org/cgi/content/full/5/7/eaaw0315/DC1

Fig. S1. Deletion of FcRL1 gene in CH27 cells and mouse with CRISPR-Cas9.
Fig. S2. Flow cytometry analysis of the expression level of BCR and FcRL1 on plasma membrane and intracellular c-Abl fusion protein.
Fig. S3. Off-target detection of the sgRNA used for knocking out FcRL1 in CH27 cells.
Fig. S4. Off-target detection of the upstream sgRNA used for knocking out FcRL1 in mouse.
Fig. S5. Off-target detection of the downstream sgRNA used for knocking out FcRL1 in mouse.
Fig. S6. FcRL1 deficiency in primary B cell intrinsically impaired the antigen binding–induced B cell activation in the absence of FcRL1 ligation.
Fig. S7. FcRL1 is passively recruited into the B cell immunological synapse upon BCR engagement in CH27-FcRL1-KO B cells expressing HA-FcRL1-YFP.
Fig. S8. Sequence alignment of the cytoplasmic tail of FcRL1.
Fig. S9. Disruption of FcRL1 gene had no effect on B cell development in FcRL1-KO mice.

REFERENCES AND NOTES

1. I. Miller, G. Hatzivassiliou, G. Cattoretti, C. Mendelsohn, R. Dalla-Favera, IRTAs: A new family of immunoglobulinlike receptors differentially expressed in B cells. *Blood* **99**, 2662–2669 (2002).
2. J. Hombach, T. Tsubata, L. Leclercq, H. Stappert, M. Reth, Molecular components of the B-cell antigen receptor complex of the IgM class. *Nature* **343**, 760–762 (1990).
3. N. E. Harwood, F. D. Batista, Early events in B cell activation. *Annu. Rev. Immunol.* **28**, 185–210 (2010).
4. M. Reth, Antigen receptor tail clue. *Nature* **338**, 383–384 (1989).
5. Y. Xu, K. W. Harder, N. D. Huntington, M. L. Hibbs, D. M. Tarlinton, Lyn tyrosine kinase: Accentuating the positive and the negative. *Immunity* **22**, 9–18 (2005).
6. J. G. Monroe, ITAM-mediated tonic signalling through pre-BCR and BCR complexes. *Nat. Rev. Immunol.* **6**, 283–294 (2006).
7. S. A. Johnson, C. M. Pleiman, L. Pao, J. Schneringer, K. Hippen, J. C. Cambier, Phosphorylated immunoreceptor signaling motifs (ITAMs) exhibit unique abilities to bind and activate Lyn and Syk tyrosine kinases. *J. Immunol.* **155**, 4596–4603 (1995).
8. T. Yasuda, T. Tezuka, A. Maeda, T. Inazu, Y. Yamanashi, H. Gu, T. Kurosaki, T. Yamamoto, Cbl-b positively regulates Btk-mediated activation of phospholipase C-γ2 in B cells. *J. Exp. Med.* **196**, 51–63 (2002).
9. T. Kurosaki, S. Tsukada, BLNK: Connecting Syk and Btk to calcium signals. *Immunity* **12**, 1–5 (2000).
10. M. Ishiai, M. Kurosaki, R. Pappu, K. Okawa, I. Ronko, C. Fu, M. Shibata, A. Iwamatsu, A. C. Chan, T. Kurosaki, BLNK required for coupling Syk to PLCγ2 and Rac1-JNK in B cells. *Immunity* **10**, 117–125 (1999).
11. T. Kurosaki, Regulation of B-cell signal transduction by adaptor proteins. *Nat. Rev. Immunol.* **2**, 354–363 (2002).
12. L. Srinivasan, Y. Sasaki, D. P. Calado, B. Zhang, J. H. Paik, R. A. DePinho, J. L. Kutok, J. F. Kearney, K. L. Otipoby, K. Rajewsky, PI3 kinase signals BCR-dependent mature B cell survival. *Cell* **139**, 573–586 (2009).
13. J. Wang, L. Xu, S. Shaheen, S. Liu, W. Zheng, X. Sun, Z. Li, W. Liu, Growth of B cell receptor microclusters is regulated by PIP_2 and PIP_3 equilibrium and Dock2 recruitment and activation. *Cell Rep.* **21**, 2541–2557 (2017).
14. P. Tolar, Cytoskeletal control of B cell responses to antigens. *Nat. Rev. Immunol.* **17**, 621–634 (2017).
15. S. J. Fleire, J. P. Goldman, Y. R. Carrasco, M. Weber, D. Bray, F. D. Batista, B cell ligand discrimination through a spreading and contraction response. *Science* **312**, 738–741 (2006).
16. L. Xu, A. Auzins, X. Sun, Y. Xu, F. Harnischfeger, Y. Lu, Z. Li, Y.-H. Chen, W. Zheng, W. Liu, The synaptic recruitment of lipid rafts is dependent on CD19-PI3K module and cytoskeleton remodeling molecules. *J. Leukoc. Biol.* **98**, 223–234 (2015).
17. M. Ono, S. Bolland, P. Tempst, J. V. Ravetch, Role of the inositol phosphatase SHIP in negative regulation of the immune system by the receptor FcγRIIB. *Nature* **383**, 263–266 (1996).
18. L. Xu, G. Li, J. Wang, Y. Fan, Z. Wan, S. Zhang, S. Shaheen, J. Li, L. Wang, C. Yue, Y. Zhao, F. Wang, J. Brzostowski, Y. H. Chen, W. Zheng, W. Liu, Through an ITIM-independent mechanism the FcγRIIB blocks B cell activation by disrupting the colocalized microclustering of the B cell receptor and CD19. *J. Immunol.* **192**, 5179–5191 (2014).
19. L. Xu, M. Xia, J. Guo, X. Sun, H. Li, C. Xu, X. Gu, H. Zhang, J. Yi, Y. Fang, H. Xie, J. Wang, Z. Shen, B. Xue, Y. Sun, T. Meckel, Y.-H. Chen, Z. Hu, Z. Li, C. Xu, H. Gong, W. Liu, Impairment on the lateral mobility induced by structural changes underlies the functional deficiency of the lupus-associated polymorphism FcγRIIB-T232. *J. Exp. Med.* **213**, 2707–2727 (2016).
20. R. S. Davis, Fc receptor-like molecules. *Annu. Rev. Immunol.* **25**, 525–560 (2007).
21. C. M. Leu, R. S. Davis, L. A. Gartland, W. D. Fine, M. D. Cooper, FcRH1: An activation coreceptor on human B cells. *Blood* **105**, 1121–1126 (2005).
22. D. Depoil, S. Fleire, B. L. Treanor, M. Weber, N. E. Harwood, K. L. Marchbank, V. L. Tybulewicz, F. D. Batista, CD19 is essential for B cell activation by promoting B cell receptor-antigen microcluster formation in response to membrane-bound ligand. *Nat. Immunol.* **9**, 63–72 (2008).
23. N. E. Harwood, F. D. Batista, New insights into the early molecular events underlying B cell activation. *Immunity* **28**, 609–619 (2008).
24. F. A. Ran, P. D. Hsu, J. Wright, V. Agarwala, D. A. Scott, F. Zhang, Genome engineering using the CRISPR-Cas9 system. *Nat. Protoc.* **8**, 2281–2308 (2013).

25. H. W. Sohn, P. Tolar, S. K. Pierce, Membrane heterogeneities in the formation of B cell receptor-Lyn kinase microclusters and the immune synapse. *J. Cell Biol.* **182**, 367–379 (2008).
26. J. Adler, I. Parmryd, Quantifying colocalization by correlation: The Pearson correlation coefficient is superior to the Mander's overlap coefficient. *Cytometry A* **77**, 733–742 (2010).
27. Z. Songyang, S. E. Shoelson, M. Chaudhuri, G. Gish, T. Pawson, W. G. Haser, F. King, T. Roberts, S. Ratnofsky, R. J. Lechleider, B. G. Neel, R. B. Birge, J. E. Fajardo, M. M. Chou, H. Hanafusa, B. Schaffhausen, L. C. Cantley, SH2 domains recognize specific phosphopeptide sequences. *Cell* **72**, 767–778 (1993).
28. P. A. Zipfel, M. Grove, K. Blackburn, M. Fujimoto, T. F. Tedder, A. M. Pendergast, The c-Abl tyrosine kinase is regulated downstream of the B cell antigen receptor and interacts with CD19. *J. Immunol.* **165**, 6872–6879 (2000).
29. D. G. Savage, K. H. Antman, Imatinib mesylate—A new oral targeted therapy. *N. Engl. J. Med.* **346**, 683–693 (2002).
30. M. Reth, Pillars article: Antigen receptor tail clue. Nature. 1989. 338: 383-384. *J. Immunol.* **192**, 4015–4016 (2014).
31. Y. Wang, S. R. Brooks, X. Li, A. N. Anzelon, R. C. Rickert, R. H. Carter, The physiologic role of CD19 cytoplasmic tyrosines. *Immunity* **17**, 501–514 (2002).
32. D. A. Tuveson, R. H. Carter, S. P. Soltoff, D. T. Fearon, CD19 of B cells as a surrogate kinase insert region to bind phosphatidylinositol 3-kinase. *Science* **260**, 986–989 (1993).
33. Y. Wang, R. H. Carter, CD19 regulates B cell maturation, proliferation, and positive selection in the FDC zone of murine splenic germinal centers. *Immunity* **22**, 749–761 (2005).
34. P. Engel, L.-J. Zhou, D. C. Ord, S. Sato, B. Koller, T. F. Tedder, Abnormal B lymphocyte development, activation, and differentiation in mice that lack or overexpress the CD19 signal transduction molecule. *Immunity* **3**, 39–50 (1995).
35. D. T. Fearon, M. C. Carroll, Regulation of B lymphocyte responses to foreign and self-antigens by the CD19/CD21 complex. *Annu. Rev. Immunol.* **18**, 393–422 (2000).
36. T. F. Tedder, L. J. Zhou, P. Engel, The CD19/CD21 signal transduction complex of B lymphocytes. *Immunol. Today* **15**, 437–442 (1994).
37. R. S. Davis, Y.-H. Wang, H. Kubagawa, M. D. Cooper, Identification of a family of Fc receptor homologs with preferential B cell expression. *Proc. Natl. Acad. Sci. U.S.A.* **98**, 9772–9777 (2001).
38. D. C. Otero, R. C. Rickert, CD19 function in early and late B cell development. II. CD19 facilitates the pro-B/pre-B transition. *J. Immunol.* **171**, 5921–5930 (2003).
39. Q. L. K. Lam, C. K. C. Lo, B.-J. Zheng, K.-H. Ko, D. G. Osmond, G. E. Wu, R. Rottapel, L. Lu, Impaired V(D)J recombination and increased apoptosis among B cell precursors in the bone marrow of c-Abl-deficient mice. *Int. Immunol.* **19**, 267–276 (2007).
40. W. Liu, T. Meckel, P. Tolar, H. W. Sohn, S. K. Pierce, Antigen affinity discrimination is an intrinsic function of the B cell receptor. *J. Exp. Med.* **207**, 1095–1111 (2010).
41. W. Liu, E. Chen, X. W. Zhao, Z. P. Wan, Y. R. Gao, A. Davey, E. Huang, L. Zhang, J. Crocetti, G. Sandoval, M. G. Joyce, C. Miceli, J. Lukszo, L. Aravind, W. Swat, J. Brzostowski, S. K. Pierce, The scaffolding protein synapse-associated protein 97 is required for enhanced signaling through isotype-switched IgG memory B cell receptors. *Sci. Signal.* **5**, ra54 (2012).
42. X. Chen, W. Pan, Y. Sui, H. Li, X. Shi, X. Guo, H. Qi, C. Xu, W. Liu, Acidic phospholipids govern the enhanced activation of IgG-B cell receptor. *Nat. Commun.* **6**, 8552 (2015).

Acknowledgments: We thank H. Qi (Tsinghua University) for material and technical support with the CRISPR-Cas9 system. We thank S. K. Pierce (National Institute of Allergy and Infectious Diseases, NIH), K. Rajewsky (Immune Regulation and Cancer, Max-Delbrück-Center for Molecular Medicine), M. Shlomchik (Yale University), T. Kurosaki (WPI Immunology Frontier Research Center, Osaka University, Japan), and H. Shinohara (WPI Immunology Frontier Research Center) for providing experimental materials. **Funding:** This work was supported by funds from the National Science Foundation China (81825010, 81730043, 81621002, and 31811540397) to W.L. and National Multiple Sclerosis Society (Career Transition Award TA 3059-A-2) to C.W. **Author contributions:** X.Z. designed and performed experiments, analyzed data, prepared figures, and wrote the paper. H.X., M.Z., A.A., X.L., and J.Y. performed experiments, analyzed data, and wrote the paper. F.W. provided reagents. C.W., Z.Y., and I.R. provided technical assistance. Q.-Z.L. and T.J.K. provided conceptual advice and revised the paper. W.L. designed and coordinated the study, provided funding, and wrote the paper. **Competing interests:** The authors declare that they have no competing interests. **Data and materials availability:** All data needed to evaluate the conclusions in the paper are present in the paper and/or the Supplementary Materials. Additional data related to this paper may be requested from the authors.

Submitted 12 November 2018
Accepted 13 June 2019
Published 17 July 2019
10.1126/sciadv.aaw0315

Citation: X. Zhao, H. Xie, M. Zhao, A. Ahsan, X. Li, F. Wang, J. Yi, Z. Yang, C. Wu, I. Raman, Q.-Z. Li, T. J. Kim, W. Liu, Fc receptor–like 1 intrinsically recruits c-Abl to enhance B cell activation and function. *Sci. Adv.* **5**, eaaw0315 (2019).